Hybrid Nanoparticles

DOI: 10.1002/ange.201008097

Simultaneous Optical Monitoring of the Overgrowth Modes of Individual Asymmetric Hybrid Nanoparticles**

Young In Yang, Eunhye Jeong, Inhee Choi, Suseung Lee, Hyeon Don Song, Kihoon Kim, Yeonho Choi, Taewook Kang,* and Jongheop Yi**

Nanoparticles that combine domains with different compositions (e.g., noble metals, iron oxide, organic compounds, or polymer) have attracted considerable interest for biomedical applications, because two or more important functions, for example, targeting, imaging, and therapy, can be combined into a single nanoparticle, and such a particle would increase the precision and efficacy of diagnosis and treatment.[1] A gold nanoparticle is well suited to the framework of multifunctional nanoparticles owing to its biocompatible surface and unique optical properties.[2] Surface conjugation with an antibody, DNA, a drug-embedded polymer, or an iron oxide moiety could enable a variety of combinations for targeting, imaging, and photothermal treatment.[3]

Many research efforts have been focused on the synthesis of these particles.[4] Some issues, such as reproducibility, uniformity in size and shape, and in-solution production, however, remain challenging, as there is a lack of information regarding the formation and overgrowth of heterogeneous nanoparticles.[5] To overcome these current synthetic limitations, the growth mechanism of these particles should be explored. This knowledge could significantly contribute to the rational design and precise fabrication of the particles. To date, only a few monitoring techniques, including in situ TEM and UV/Vis spectroscopy, have been used to study the growth mechanism of homogeneous nanoparticles.[6]

Herein, we show that by exploiting single-particle scattering spectra, mechanisms underlying the overgrowth of Au on dimeric gold/polystyrene (gold/PS) nanoparticles can be inferred, which are largely hidden in UV/Vis spectroscopy and TEM owing to ensemble averaging and two-dimensional image projection (Figure 1). Since the UV/Vis absorption spectrum is obtained by the ensemble signal measurement of multiple dimers in solution, it is not easy to address the issue of the precise growth mechanism for individual dimers. In comparison, scattering spectra based on individual particles provide more precise information concerning the growth mechanism. During overgrowth of Au, distinct patterns in scattering spectra of single dimeric particles were differentiated. We also propose an overgrowth mechanism that

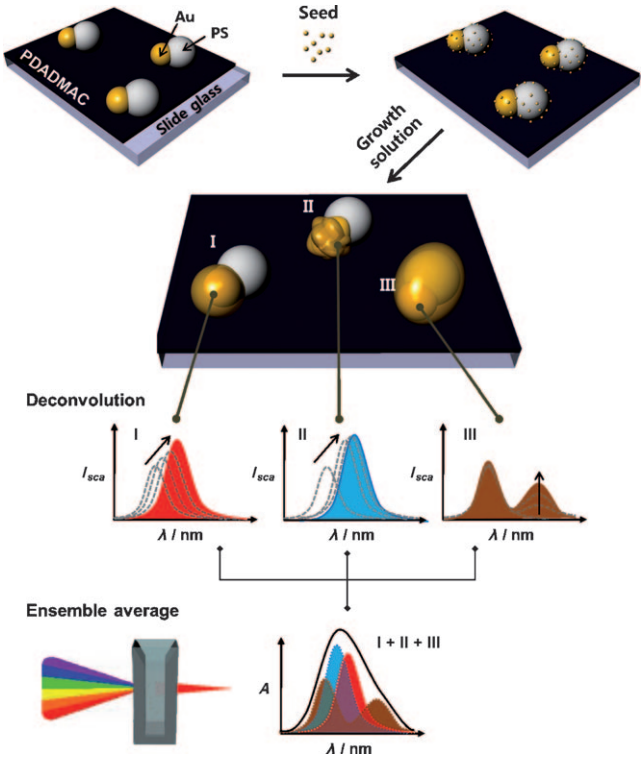

Figure 1. A cartoon showing the growth of a gold/PS dimer with the reduction of Au^{+} ions on its surface and correlation of the predicted UV/Vis absorption with scattering spectra for single hybrid dimers.

[*] Y. I. Yang,[+] Dr. I. Choi, S. Lee, H. D. Song, Prof. J. Yi
World Class University Program of Chemical Convergence for Energy & Environment, Institute of Chemical Processes
School of Chemical and Biological Engineering
Seoul National University, Seoul, 151-744 (Republic of Korea)
E-mail: jyi@snu.ac.kr

E. Jeong,[+] K. Kim, Prof. T. Kang
Department of Chemical and Biomolecular Engineering
Sogang University, Seoul, 121-742 (Republic of Korea)
E-mail: twkang@sogang.ac.kr

Prof. Y. Choi
Department of Biomedical Engineering
Korea University, Seoul, 136-703 (Republic of Korea)
E-mail: yeonhochoi@korea.ac.kr

[+] These authors contributed equally to the work.

[**] This work was supported by a grant No. 101-082-032 from the Ministry of Environment, Korea, WCU (World Class University) program through the Korea Science and Engineering Foundation funded by the Ministry of Education, Science and Technology (R31-10013), and a grant (code No. 2010K000352) from "Center for Nanostructured Materials Technology" under "21st Century Frontier R&D Programs" of the Ministry of Education, Science and Technology, Korea. It was also supported by the Sogang University research grant, the Korea Research Foundation Grant funded by the Korea Government (MOEHRD, Basic Research Promotion Fund) (KRF-2008-331-D00134). Y.C. also acknowledges financial support from the Basic Science Program through the National Research Foundation of Korea (NRF) funded by the Ministry of Education, Science, and Technology (Grant No. 2010-0022077), Korea University (Grant No. K1000681).

Supporting information for this article is available on the WWW under http://dx.doi.org/10.1002/anie.201008097.

corresponds to each pattern. Gold/PS dimeric nanoparticles were selected as a model system because the combination of gold and polymer moieties would be useful in terms of multifunctional capability and further modification.[2d,7] The overgrowth of Au on a single gold/PS nanoparticle was monitored by dark-field microscopy[8] in association with a homemade microfluidic system (Figure 2).

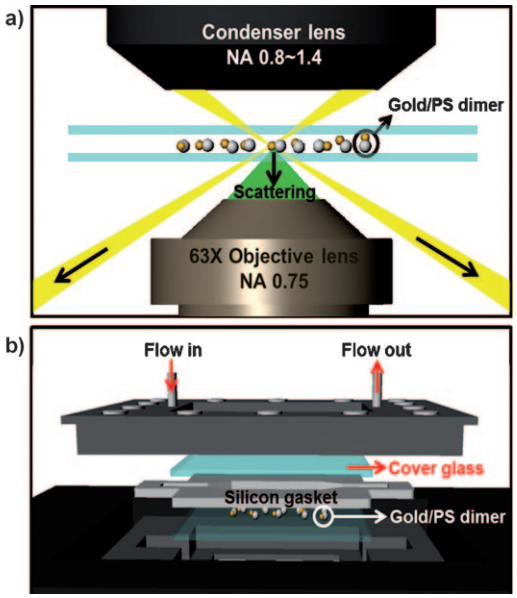

Figure 2. a) Schematic illustration of the simultaneous optical monitoring of the overgrowth of a single gold/PS dimer. b) A homemade microfluidic system combined with dark-field microscopy for real-time monitoring under the reaction conditions.

Gold/PS dimers were synthesized as reported.[7] As shown in Figure S1 in the Supporting Information, the prepared dimers consist of 50 nm layers of gold and 75 nm layers of PS. Prior to the overgrowth of Au, the gold/PS nanoparticles were attached to the surface of a cover glass by electrostatic attraction (Figure S2 in the Supporting Information). The cover glass was first functionalized with poly(diallyldimethylammonium chloride) (PDADMAC), a positively charged polyelectrolyte, and subsequently the negatively charged gold/PS nanoparticles were immobilized. Note that the gold/PS dimer is negatively charged, owing to the presence of carboxylic groups on the gold portion and sulfonate groups on the PS portion. To avoid the nucleation of Au in solution and to facilitate the selective overgrowth of Au on the surface of the nanoparticles, cetyltrimethylammonium bromide (CTAB)-capped gold seeds (ca. 4 nm) were attached to the nanoparticles.

The final cover glass was integrated with a homemade microfluidic system (Figure 2b). During overgrowth, time-resolved scattering spectra of individual dimeric nanoparticles were collected by means of a dark-field microscopy system. To clearly observe overgrowth on individual gold/PS nanoparticles, the crystallization of CTAB and nucleation of Au in solution must be avoided. The concentrations of Au^{3+}, CTAB, Ag^{+}, and ascorbic acid in the growth solution were carefully selected to minimize unwanted nucleation in solution. Moreover, the overgrowth reaction in the flow chamber was maintained at 25 °C to prevent the crystallization of excess CTAB in the growth solution.

Since a change in the size and shape of a gold nanoparticle is directly related to different localized surface plasmon polaritons, in situ observation of the scattering profile permits estimation of morphological changes of the gold nanoparticle as well as of the kinetics during overgrowth.[9] By analyzing the time-resolved scattering spectra of 20 different individual nanoparticles, we found that three different growth modes existed, even under identical overgrowth conditions. The representative spectral changes for each mode are shown in Figure 3. In mode I (11 out of 20 spectra), the scattering intensity increases and the plasmon resonance frequency is red-shifted with increasing reaction time. Patterns similar to this scattering profile can be found in cases of growth of single spherical nanoparticles. When light scattering from PS is neglected owing to the four or five orders of magnitude

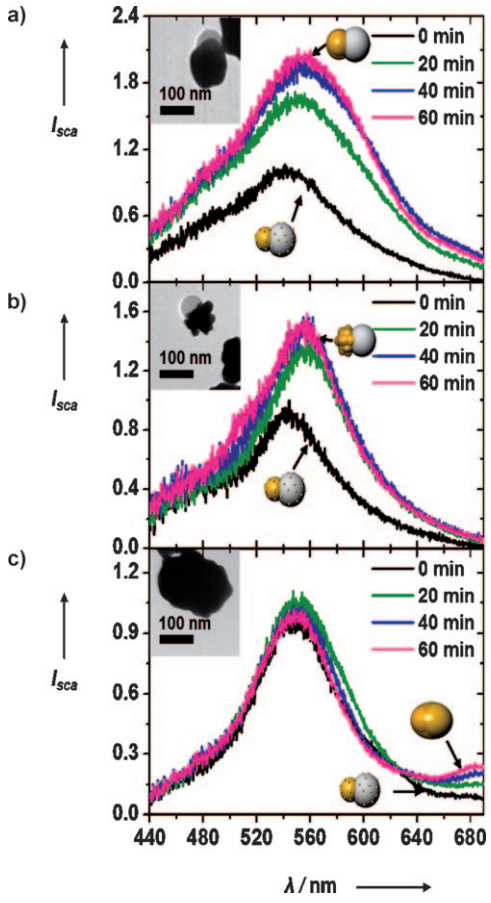

Figure 3. Representative spectral changes for the three different growth modes observed under identical overgrowth conditions. Each inset shows the TEM image of a final overgrown structure for each growth mode. a) Mode I: The scattering intensity increases and the plasmon resonance frequency is red-shifted with increasing reaction time. b) Mode II: Analogous to mode I, but about 75% of the total change takes place within 20 min. c) Mode III: The scattering peak maxima (around 550 nm) are nearly unchanged, but a new scattering resonant peak appears at a longer wavelength (around 680 nm), and its intensity gradually increases with reaction time.

differences in Rayleigh scattering cross sections between gold and PS,[10] it appears that most of the Au^+ ions contribute to selective growth on the gold portion, and the size of the gold portion grows gradually, as shown in the inset TEM image of Figure 3a. Mode II (5 out of 20 spectra) is analogous to mode I, and the scattering spectra show an increase in intensity and a red shift in the resonance frequency during overgrowth. However, about 75% of the total changes occur within 20 min, whereas mode I shows a relatively gradual change over a period of 60 min. The more rapid change associated with mode II suggests that during reaction, the overgrowth of Au proceeds over the entire surface of the gold portion, thus leading to the symmetrical overgrowth on the gold portion, as evidenced by the maintenance of a single Gaussian shape in the scattering spectra. However, instead of a larger spherical shape, an extended shape resembling a fin or spike is produced, as shown in the inset TEM image of Figure 3b, leading to a more rapid reaction rate than in mode I. Unlike growth modes I and II, the scattering peak maxima (around 550 nm) and intensities remain nearly constant with increasing reaction time in mode III (4 out of 20 spectra). However, in mode III, a new scattering resonant peak is observed at a longer wavelength (around 680 nm), and its intensity gradually increases as overgrowth proceeds. This behavior can be attributed the generation of a second resonance peak corresponding to asymmetric growth from a gold/PS dimer. Consequently, the final structure has an elliptical shape in which the PS portion is fully covered by gold (Figure 3c, inset).

Figure 4 demonstrates the kinetic change of the resonance frequency, intensity ratio ($I_{680\,nm}/I_{550\,nm}$), and equivalent radius in detail. As shown in Figure 4a, the peak shifts of the resonance frequency with respect to the reaction time are also different among the three modes. In modes I and II, the position of the resonance peak shifted by about 10 nm to a longer wavelength, but there was no significant change in mode III. In mode III, instead, a second peak appeared at about 680 nm (see Figure 3c). We compared the intensity ratio of the second resonance peak to the first one (Figure 4b). During overgrowth, the ratio showed an 18% decrease in modes I and II, which resulted from the increased intensity of the first peak. In contrast, it increased by 48% in mode III owing to a significant increase in the second peak. Therefore, the striking contrast in the intensity ratio reveals that more than one collective oscillation exists.

To more quantitatively examine each overgrowth mode, we calculated the equivalent radius from the change in measured intensity, assuming a spherical structure. Since the change in the scattering intensity (I_{sca}) is proportional to the sixth power of the particle diameter [D, Eq. (1)]:[9a,11]

$$I_{sca} \propto D^6 \quad (1)$$

the equivalent radius can be related to the scattering intensities using Equation (2):

$$R_{eq} = R_0(I_{(t)}/I_0)^{1/6} \quad (2)$$

where R_{eq} is the equivalent radius, R_0 is the initial radius of a gold nanoparticle ($R_0 = 50$ nm), and I_0 is the initial scattering intensity. Furthermore, for mode III, we take the averaged values for the two radii, as estimated from the two resonance peaks (see Figure S3 in the Supporting Information). In modes I and II, the equivalent radii gradually increase up to 27 nm within a period of 15 min. However, the radius in mode II is saturated after 15 min, while mode I shows a gradual increase up to 28 nm over a period of 60 min. In contrast, in the case of overgrowth mode III, the equivalent radius increases to 30 nm, which corresponds to 44% and 64% larger volume than the particles resulting from growth modes I and II, respectively. More experimental and theoretical studies to investigate the population of each overgrowth mode and factors that dominate a specific overgrowth mode are currently under investigation.

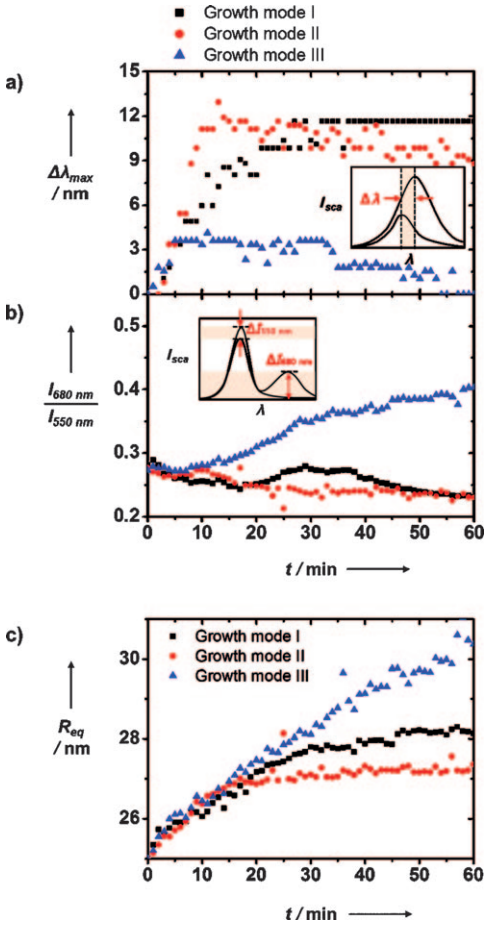

Figure 4. Kinetic changes of resonance frequency, intensity ratio ($I_{680\,nm}/I_{550\,nm}$), and equivalent radius. a) Plots of the shift of peak maximum in the scattering spectra as a function of overgrowth time. In modes I and II, the resonance peak is red-shifted by about 10 nm, while there was no significant change in mode III. b) The scattering intensity ratio for the two resonance peaks (around 550 nm and 680 nm, respectively). Unlike growth modes I and II, $I_{680\,nm}/I_{550\,nm}$ increases by 48% in mode III, owing to the significant increase in the longitudinal plasmon band (around 680 nm). Insets in (a) and (b) describe the method used for replotting from the original spectra. c) Time-dependent changes in equivalent radius calculated using Equation (2). In growth mode III, the equivalent volume is 44 and 64% larger than those for growth modes I and II.

In conclusion, by exploiting the time-resolved Rayleigh scattering spectra of single nanoparticles, the mechanisms underlying the overgrowth of Au on individual dimeric gold/PS nanoparticles can be revealed. It would not be possible to accomplish this aim using UV/Vis spectroscopy and TEM owing to ensemble averaging and the fact that two-dimensionally projected images are produced in the case of TEM. During the overgrowth of Au, three distinct patterns in the scattering spectra of individual dimeric particles can be differentiated. In mode I, the scattering intensity increases and the plasmon resonance frequency is red-shifted with increasing reaction time, thus suggesting that most of the Au^{+} ions are selectively nucleated on the gold portion, and the size of the gold portion grows in a symmetrical manner. Compared with mode I, the more rapid change in the intensity and resonance frequency in mode II suggests that, during overgrowth, the nucleation of Au leads the production of gold/PS nanoparticles with an extended shape resembling a fin or spike. Unlike growth modes I and II, a new scattering resonant peak at longer wavelength is observed (around 680 nm) in mode III, and its intensity gradually increases as overgrowth proceeds. We attribute the generation of the second resonance peak to asymmetric growth (e.g., elliptical shape) originating from a single gold/PS heterogeneous nanoparticle. We expect that these results can directly provide a better understanding of the growth mechanism and help overcome current limitations in the synthesis of nanoparticles.

Received: December 22, 2010
Published online: April 14, 2011

Keywords: dark-field microscopy · nanoparticles · organic–inorganic hybrid composites · overgrowth · real-time monitoring

[1] a) J. Kim, Y. Piao, T. Hyeon, *Chem. Soc. Rev.* **2009**, *38*, 372 – 390; b) S.-H. Hu, X. Gao, *J. Am. Chem. Soc.* **2010**, *132*, 7234 – 7237; c) J. Gao, H. Gu, B. Xu, *Acc. Chem. Res.* **2009**, *42*, 1097 – 1107; d) L. Wang, J. Bai, Y. Li, Y. Huang, *Angew. Chem.* **2008**, *120*, 2473 – 2476; *Angew. Chem. Int. Ed.* **2008**, *47*, 2439 – 2442; e) S. T. Selvan, P. K. Patra, C. Y. Ang, J. Y. Ying, *Angew. Chem.* **2007**, *119*, 2500 – 2504; *Angew. Chem. Int. Ed.* **2007**, *46*, 2448 – 2452; f) W. Shi, H. Zeng, Y. Sahoo, T. Y. Ohulchanskyy, Y. Ding, Z. L. Wang, M. Swihart, P. N. Prasad, *Nano Lett.* **2006**, *6*, 875 – 881; g) D. Ma, J. Guan, S. Dénommée, G. Enright, T. Veres, B. Simard, *Chem. Mater.* **2006**, *18*, 1920 – 1927; h) X. Gao, Y. Cui, R. M. Levenson, L. W. K. Chung, S. Nie, *Nat. Biotechnol.* **2004**, *22*, 969 – 976.

[2] a) Y. Choi, Y. Park, T. Kang, L. P. Lee, *Nat. Nanotechnol.* **2009**, *4*, 742 – 746; b) G. L. Liu, Y.-T. Long, Y. Choi, T. Kang, L. P. Lee, *Nat. Methods* **2007**, *4*, 1015 – 1017; c) T. Kang, S. Hong, I. Choi, J. J. Sung, Y. Kim, J.-S. Hahn, J. Yi, *J. Am. Chem. Soc.* **2006**, *128*, 12870 – 12878; d) L. Y. Wu, B. M. Ross, S. Hong, L. P. Lee, *Small* **2010**, *6*, 503 – 507.

[3] a) L. Tang, L. Liu, H. B. Elwing, *J. Biomed. Mater. Res.* **1998**, *41*, 333 – 340; b) C. Loo, A. Lowery, N. Halas, J. West, R. Drezek, *Nano Lett.* **2005**, *5*, 709 – 711; c) J. L. West, N. J. Halas, *Curr. Opin. Biotechnol.* **2000**, *11*, 215 – 217.

[4] a) C. S. Levin, C. Hofmann, T. A. Ali, A. T. Kelly, E. Morosan, P. Nordlander, K. H. Whitmire, N. J. Halas, *ACS Nano* **2009**, *3*, 1379 – 1388; b) H.-M. Song, Q. Wei, Q. K. Ong, A. Wei, *ACS Nano* **2010**, *4*, 5163 – 5173; c) J.-s. Choi, Y.-w. Jun, S.-I. Yeon, H. C. Kim, J.-S. Shin, J. Cheon, *J. Am. Chem. Soc.* **2006**, *128*, 15982 – 15983.

[5] a) I. Jen-la Plante, S. E. Habas, B. D. Yuhas, D. J. Gargas, T. Mokari, *Chem. Mater.* **2009**, *21*, 3662 – 3667; b) S. E. Habas, H. Lee, V. Radmilovic, G. A. Somorjai, P. Yang, *Nat. Mater.* **2007**, *6*, 692 – 697; c) F. R. Fan, D. Y. Liu, Y. F. Wu, S. Duan, Z. X. Xie, Z. Y. Jiang, Z. Q. Tian, *J. Am. Chem. Soc.* **2008**, *130*, 6949 – 6951; d) W. Ni, X. Kou, Z. Yang, J. Wang, *ACS Nano* **2008**, *2*, 677 – 686; e) K. Sohn, F. Kim, K. C. Pradel, J. Wu, Y. Peng, F. Zhou, J. Huang, *ACS Nano* **2009**, *3*, 2191 – 2198; f) H.-L. Wu, C.-H. Chen, M. H. Huang, *Chem. Mater.* **2008**, *21*, 110 – 114; g) X. Kou, S. Zhang, Z. Yang, C.-K. Tsung, G. D. Stucky, L. Sun, J. Wang, C. Yan, *J. Am. Chem. Soc.* **2007**, *129*, 6402 – 6404; h) D. Seo, C. I. Yoo, J. C. Park, S. M. Park, S. Ryu, H. Song, *Angew. Chem.* **2008**, *120*, 775 – 779; *Angew. Chem. Int. Ed.* **2008**, *47*, 763 – 767; i) T. K. Sau, A. L. Rogach, *Adv. Mater.* **2010**, *22*, 1781 – 1804.

[6] a) H. Zheng, R. K. Smith, Y.-w. Jun, C. Kisielowski, U. Dahmen, A. P. Alivisatos, *Science* **2009**, *324*, 1309 – 1312; b) J. Boleininger, A. Kurz, V. Reuss, C. Sonnichsen, *Phys. Chem. Chem. Phys.* **2006**, *8*, 3824 – 3827.

[7] A. Ohnuma, E. C. Cho, P. H. C. Camargo, L. Au, B. Ohtani, Y. Xia, *J. Am. Chem. Soc.* **2009**, *131*, 1352 – 1353.

[8] H. Song, I. Choi, Y. Yang, S. Hong, S. Lee, T. Kang, J. Yi, *Nanotechnology* **2010**, *21*, 145501.

[9] a) C. F. Bohren, D. R. Huffman, *Absorption and Scattering of Light by Small Particles*, Wiley-VCH, New York, **1983**; b) S. Berciaud, L. Cognet, P. Tamarat, B. Lounis, *Nano Lett.* **2005**, *5*, 515 – 518; c) B. Nikoobakht, M. A. El-Sayed, *Chem. Mater.* **2003**, *15*, 1957 – 1962.

[10] a) I. H. Chou, M. Benford, H. T. Beier, G. L. Coté, M. Wang, N. Jing, J. Kameoka, T. A. Good, *Nano Lett.* **2008**, *8*, 1729 – 1735; b) N. Del Fatti, D. Christofilos, F. Vallee, *Gold Bull.* **2008**, *41*, 147 – 158; c) C. Stevenson, T. Vo-Dinh, *Modern Techniques in Raman Spectroscopy* (Eds: J. J. Laserna), Wiley-VCH, Weinheim, **1996**, pp. 1 – 39.

[11] a) L. Cognet, S. Berciaud, D. Lasne, B. Lounis, *Anal. Chem.* **2008**, *80*, 2288 – 2294; b) R. C. Tolman, R. H. Gerke, A. P. Brooks, A. G. Herman, R. S. Mulliken, H. D. Smyth, *J. Am. Chem. Soc.* **1919**, *41*, 575 – 587; c) C. Novo, A. M. Funston, P. Mulvaney, *Nat. Nanotechnol.* **2008**, *3*, 598 – 602.

